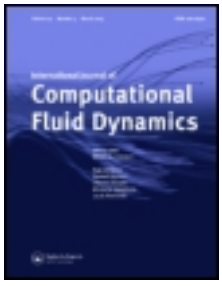

International Journal of Computational Fluid Dynamics
Publication details, including instructions for authors and subscription information:
http://www.tandfonline.com/loi/gcfd20

CFD application to oceanic mixed layer sampling with Lagrangian platforms

Tamay M. Özgökmen [a] & Paul F. Fischer [b]

[a] Rosenstiel School of Marine and Atmospheric Science, University of Miami, Florida, USA

[b] Mathematics and Computer Science Division, Argonne National Laboratory, Illinois, USA

Available online: 21 May 2012

To cite this article: Tamay M. Özgökmen & Paul F. Fischer (2012): CFD application to oceanic mixed layer sampling with Lagrangian platforms, International Journal of Computational Fluid Dynamics, DOI:10.1080/10618562.2012.668888

To link to this article: http://dx.doi.org/10.1080/10618562.2012.668888

International Journal of Computational Fluid Dynamics
2012, 1–12, i*First* article

Taylor & Francis
Taylor & Francis Group

CFD application to oceanic mixed layer sampling with Lagrangian platforms

Tamay M. Özgökmen[a]* and Paul F. Fischer[b]

[a]*Rosenstiel School of Marine and Atmospheric Science, University of Miami, Florida, USA;* [b]*Mathematics and Computer Science Division, Argonne National Laboratory, Illinois, USA*

(*Received 16 June 2011; final version received 9 February 2012*)

Frontal adjustment and restratification in oceanic mixed layers is one of the processes that is considered to be important in the ocean's multi-scale energy transfer, biogeochemical transport, air–sea interaction, acoustic propagation and naval operations. We summarise a CFD-based modelling approach to sample processes at an idealised mixed layer base using passive scalars and particles, given a subset of realistic constraints on these resources in field experiments. The results emphasise the effectiveness of Lagrangian platforms, in particular passive particles, for sampling rapidly evolving submesoscale oceanic fields.

Keywords: ocean mixing; ocean sampling; Lagrangian transport; tracers; relative dispersion

1. Introduction

1.1. Importance

Oceanic mixed layers are important for several reasons. First, the most pronounced and energetic eddies and jets in the ocean circulation have a scale on the order of the Rossby deformation scale, $O(10^4)$m (so-called mesoscale range), while viscous dissipation of kinetic energy takes place at scales on the $O(10^{-2})$m. Since the ocean is a forced-dissipative system, it is important to know how the energy driving the ocean circulation is dissipated, for reliable forecasts of the ocean state, and the climate. The potential routes to dissipation can be classified into three (Müller *et al*. 2005): (i) the ocean's internal gravity waves can interact with mesoscale motions and catalyse a cascade of their energy to dissipation scales; (ii) balanced mesoscale flows can become unstable and initiate a down-scale energy cascade and (iii) dissipation can take place by flow interactions with complex, rough bathymetry. Little is known about processes in the intermediate, or submesoscale range (Wunsch and Ferrari 2004). The submesoscale range is generally characterised by coherent features in the spatial scale range of 10^2 m to 10^4 m and an eddy turn over time scale of the order of days (Thomas *et al*. 2008). It is thought that instabilities in the mixed layer may serve as a fundamental link between mesoscales and small scales (Boccaletti *et al*. 2007, Fox-Kemper *et al*. 2008), and could be important in order to construct the full picture of oceanic multi-scale turbulent interactions (McWilliams 2008). The generation of submesoscale flows is an interesting problem because the behaviour of flows in geostrophic balance in the high-aspect ratio of ocean domains tends to be analogous to two-dimensional (2D) turbulence, where the energy cascade is primarily toward larger scales, namely away from submesoscales. Second, vertical biogeochemical transport due to submesoscale filaments created by intermittent turbulent events can be as much as those associated with mesoscale transport events in the ocean (Mahadevan and Tandon 2006, Klein and Lapeyre 2009). Third, these processes are of significant importance for naval operations, navigation, submerged equipment such as submarines, acoustic propagation and transport of mines. For these reasons, the US Office of Naval Research (ONR) formed a team of investigators to model and observe upper ocean lateral mixing processes. These processes are likely to include mixed layer instabilities, which have not been observed before (to the knowledge of the authors). One of the ONR field experiments involves three ships, an airplane and many observational platforms, and it is one the most comprehensive observational cruises in recent times.

In this manuscript, we present a short overview of modelling and observational approaches for submesoscale ocean flows, as well as a computationally demanding mixed layer dynamics study using a CFD code, subject to sampling constraints of ocean experiments.

1.2. Considerations on modelling approaches for submesoscale ocean flows

Traditional ocean general circulation models (OGCMs) have the advantage that they are already

*Corresponding author. Email: tozgokmen@rsmas.miami.edu

ISSN 1061-8562 print/ISSN 1029-0257 online

http://dx.doi.org/10.1080/10618562.2012.668888
http://www.tandfonline.com

configured at the global scale, as well as for specific ocean basins by national operational centers, such as Naval Research Laboratory (NRL) and National Center for Environmental Prediction (NCEP)[1], with mesh spacings going down to about 5 km. OGCMs can also be set up for regional simulations at finer resolutions (Capet *et al*. 2008). The primary advantage of these approaches is that the dynamics of the general circulation and mesoscale features such as jets and eddies are well captured. These OGCMs contain realistic forcing, domain geometry, and assimilate ocean data.

There are however several disadvantages of OGCMs for simulating submesoscale flows. First, the equation set (so-called primitive equations (PE)) contains the hydrostatic approximation, which is justified by the high aspect ratio between horizontal and vertical domain dimensions. The hydrostatic approximation becomes invalid for scales below approximately 1 km (Kantha and Clayson 2000), thus within the submesoscale range. The breakdown of the hydrostatic approximation creates two types of errors in OGCMs. Internal waves are prominent features in the ocean with well-known dispersion relations and characteristics (Garrett and Munk 1972). It is known that hydrostatic models cannot produce the correct dispersion for non-linear internal waves, leading to unrealistically fast propagating waves (Scotti and Mitran 2008). Also, the overturning of density surfaces by Kelvin-Helmholtz instabilities, which are one of the primary mechanisms responsible for mixing in the ocean, cannot be explicitly captured with hydrostatic models. In fact, the accuracy of hydrostatic models can substantially degrade with finer resolution at such scales (Chang *et al*. 2005). Inclusion of a non-hydrostatic pressure solver in hydrostatic OGCMs requires a substantial change in these codes (Scotti and Mitran 2008).

Second, for the reasons described above, OGCMs contain parameterisations for mixing and dissipation (but not for dispersion, to the knowledge of the authors). These parameterisations may range from algebraic models to second-order turbulence closures (Large 1998). One challenge with algebraic closures is that they can contain dimensional parameters that need to be tuned for different flow problems (Chang *et al*. 2005). The turbulence closures have been imported from the engineering community and further developed for stratified oceanic flows (Mellor and Yamada 1982, Kantha and Clayson 1994, Burchard and Baumert 1995, Burchard and Bolding 2001, Canuto *et al*. 2001, Baumert and Peters 2004, Baumert *et al*. 2005, Umlauf and Burchard 2005, Warner *et al*. 2005, Canuto *et al*. 2007). They have been shown to work well in challenging ocean mixing problems (e.g. Ilicak *et al*. 2008). But perhaps they require more extensive evaluation as more comprehensive ocean data become available. Also, given that the hydrostatic approximation changes the vertical momentum balance, turbulence closures are applied only in the vertical direction. This has created a disconnect between horizontal and vertical closure schemes.

Third, there are challenges with data assimilation. Assimilation can influence conservation laws. In addition, it is not clear that assimilating data that contain much higher spatial resolution than the OGCMs, or simply point measurements on 5–10 km grids would enhance the realism of the model for submesoscale processes. Finally, the prevailing OGCMs are based on second order numerics, thereby requiring more mesh points for convergence than higher order methods (Deville *et al*. 2002). Given that submesoscale processes are expected to be captured near the highest resolved wave number range in OGCMs, it becomes likely that numerical dissipation and dispersion errors could influence submesoscale flow behaviour.

As such, it is beneficial to consider methods developed in the CFD community for simulating submesoscale flows. While these models are typically not configured to incorporate the large-scale realism of OGCMs, they offer high numerical accuracy, scalability, adaptive and/or unstructured meshes, and integrate the well-established Navier–Stokes or Boussinesq equations (BE) of motion. In that sense, they address many of the issues that create challenges for OGCMs outlined above. Nevertheless, not all CFD methods are appropriate for oceanic problems. The large Reynolds numbers in ocean flows prohibit the direct numerical simulation (DNS), in which all degrees of freedom are computed. Reynolds averaged Navier Stokes (RANS, Wilcox 1998) codes are computationally efficient, but raise several questions. First, the decomposition of the flow field into a mean and fluctuating component creates some ambiguity for transient flows, as in the case of mixed layer instability. Second, many RANS closures rely on the eddy viscosity paradigm, or forward cascade of energy, which is not always valid in the presence of stratification, and, in particular, rotation (Vallis 2006). An alternate approach is the large eddy simulation (LES, Ferziger 2005), which lies in between the extremes of DNS, in which all turbulence is resolved, and RANS, in which all turbulence is modelled. In regards to the numerical method, the spectral element method (SEM), which combines the geometrical flexibility of finite element method (FEM) with the numerical accuracy of spectral models (Patera 1984, Maday and Patera 1989), seems to be ideally suited for submesoscale oceanic flows.

Here, we employ Nek5000, which is a mature DNS and LES model based on the SEM developed by P.F. Fischer[2] and colleagues. It has been used in ocean related research (Özgökmen *et al*. 2004a,b, 2006, Chang *et al*. 2005, Xu *et al*. 2006, Özgökmen *et al*. 2007, Özgökmen and Fischer 2008, Ilicak *et al*. 2009; Özgökmen *et al*. 2009a,b) and most recently in an investigation of mixed layer instability (Özgökmen *et al*. 2011).

1.3. Considerations on observational approaches for submesoscale ocean flows

Submesoscale flows would ideally require 4D (x,y,z,t) sampling of velocity and density fields. But, the large volume of water makes representative measurements a difficult, or even a daunting challenge (Sanford *et al*. 2011). Traditional instruments such as current meter moorings collect fixed point measurements of horizontal velocity components, and are not well suited for flows with a high degree of spatial structure. Shipboard instruments for measuring density fields (such as conductivity temperature depth (CTD)) and velocity (such as acoustic Doppler current profiler (ADCP)) allow flexibility in spatial sampling, but they are slaved to the location of the ship, thereby requiring multiple ships for simultaneous surveys. Vertically profiling autonomous instruments such as gliders (Webb *et al*. 2001) offer a cost-efficient alternative to ships for long-term monitoring of water properties. But profiling instruments create a compromise between vertical and horizontal coverage. Current meters installed on autonomous vehicles measure only the relative velocity of the device through the surrounding water. Also, rapidly moving internal wave displacements create aliasing errors in glider profiles, since each of the vertical cycles can take many hours to complete.

There are two remote sensing approaches that offer horizontal snapshots of ocean fields. The first is satellite or aircraft based sensors. Altimeters detect sea surface height anomaly, from which an estimate of ocean currents can be obtained through the assumption of geostrophic momentum balance. Nevertheless, current satellite products[3] offer only mesoscale-resolving capability. Even when higher resolution products become available, errors associated with the Earth's gravity anomalies and waves can become comparable to the ocean's surface topography signal created by submesocale flows. Ocean colour sensors[4] reveal significantly more detail at much high resolutions. Nevertheless, they do not detect any of the primary variables of the equations of motion, but rather chlorophyll, which is mostly limited to coastal regions and represents a depth-averaged distribution of a quasi-passive scalar field.

High frequency (HF) radar is an exciting tool with spatial and temporal resolutions down to about 250 m and 15 min, respectively, providing true snapshots of surface velocity fields over length scales of 10–100 km (Steward and Joy 1974, Paduan and Rosenfeld 1996, Kaplan *et al*. 2005, Shay *et al*. 2007). In fact, submesoscale features have been detected by an HF radar (Shay *et al*. 2003). These instruments are becoming widely used in coastal experiments (Haza *et al*. 2010). Nevertheless, HF radars are limited to coastal zones and surface flows at the present moment.

There are two observational techniques that are quite well suited for sampling submesoscale flows. The first is the use of Lagrangian particles. While Lagrangian drifters and floats have been used in oceanography for a long time to detect ocean currents (Davis 1985, Lumpkin and Pazos 2007), it is only recently that simultaneous launches of drifter clusters are being used as a technique to infer measures of multi-scale stirring in the underlying fluid (Koszalka *et al*. 2009, Lumpkin and Elipot 2010, Schroeder *et al*. 2011). The second is upper ocean dye release that can be detected using airborne laser (Sundermeyer *et al*. 2007), or LIDAR. Since the LIDAR is able to sample with approximately 200 m swath from an airplane flying with 100 m/s, it is capable of providing truly synoptic horizontal fields of upper ocean tracer concentration. Both platforms are essentially Lagrangian sampling methods that avoid many of the aliasing errors of some other approaches.

1.4. Objectives

Our main goal here is to create fields of mixed layer instability using a CFD code, and then examine the effectiveness of passive tracers and drifters in sampling these submesoscale flows. This study is a continuation of a recent effort (Özgökmen *et al*. 2011), but differs in that we consider sampling strategies subject to the following experimental constraints:

(a) The flows of interest take place inside mixed layers that are about 25 m deep, when compared to the lateral size of interest of 10^4 m. Modelling of flows with such high geometric aspect ratio of 1/400 demands schemes with low numerical dissipation and the use of high Peclet numbers in order to avoid an unrealistic conversion of available potential energy driving the system to background potential energy by spurious mixing, instead of kinetic energy via flow instabilities.
(b) The tracer patches are likely to be approximately 500 m long, 50 m wide and 2 m thick (all dimensions are estimates within a factor of about four). The tracer is to be injected at the

mixed layer base. This is mainly to reduce the effects of the diurnal cycle and of wind-driven flows near the surface on tracer evolution.

(c) Due to the decay rate of fluorescein needed for airborne detection of the dye by laser, the LIDAR (Sundermeyer *et al.* 2007) observation period is limited to 36 h, while other dye sampling can last up to 120 h.

(d) About 18 drifters are available with a temporal sampling of 30 min for a total period of about 30 days.

These constraints are by no means the only ones that will be encountered in the field. Here, we will assume that there are no spatial or temporal errors in observing the dye or drifters, and that the velocity field is frozen during the period of launching the observational assets. Surface or drogued drifters are subject to position errors of about 10 m (or more) via the global positioning system as well as slippage (Ohlmann *et al.* 2005). As such, the assumption of no spatial and temporal errors in drifter observations is a strong one and this topic can benefit from investigation in the near future.

2. Model setup and parameters

Nek5000 is configured to solve the following equation set:

$$\frac{D\overline{\mathbf{u}}}{Dt} = Ro_H^{-1}\,\hat{\mathbf{z}}\times\overline{\mathbf{u}} - \nabla\bar{p} - Fr^{-2}\,\overline{\rho'}\,\hat{\mathbf{z}} + Re^{-1}\nabla^2\overline{\mathbf{u}} - \nabla\cdot\tau\,, \tag{1}$$

$$\nabla\cdot\overline{\mathbf{u}} = 0\,, \tag{2}$$

$$\frac{D\overline{\rho'}}{Dt} = Pe^{-1}\nabla^2\overline{\rho'} - \nabla\cdot\sigma\,, \tag{3}$$

$$\frac{DC}{Dt} = Pe^{-1}\nabla^2 C\,, \tag{4}$$

$$\frac{d\mathbf{x}}{dt} = \overline{\mathbf{u}}\,, \tag{5}$$

where the variables are the velocity field $\mathbf{u}$, pressure p, density perturbation ρ', passive scalar field C and passive particle positions $\mathbf{x}$. The non-dimensional parameters are the Reynolds number $Re = U_0H/\nu$, the Peclet number $Pe = U_0H/\kappa$, the Froude number $Fr = U_0/(N/H)$, and the vertical Rossby number $Ro_H = U_0/(fH) = aRo$, where $Ro = U_0/(fL)$ is the Rossby number and $a = L/H$ the ratio of horizontal and vertical domain sizes. U_0 is the flow speed scale, ν is the kinematic viscosity, κ is the molecular diffusivity, g is the gravitational acceleration, ρ_0 is the fluid density, N is the buoyancy frequency, f is the Coriolis frequency, $\hat{\mathbf{z}}$ is the unit vector in the vertical direction. Not all scales of motion are resolved, but consistent with LES formalism, it is assumed that the restriction of the computed fields to the numerical grid constitutes the convolution procedure leading to spatially filtered variables $\overline{\mathbf{u}}$, $\overline{\rho'}$ and $\bar{p}$. A dynamic Smagorinsky model is used for the subgrid-scale stress tensor $\tau = \overline{\mathbf{u}\mathbf{u}} - \overline{\mathbf{u}}\,\overline{\mathbf{u}} = \tau = -2\,(c_{ds}\delta)^2\;|\nabla^s\overline{\mathbf{u}}|\,\nabla^s\overline{\mathbf{u}}$, where $\nabla^s\overline{\mathbf{u}} := (\nabla\overline{\mathbf{u}} + \nabla\overline{\mathbf{u}}^T)/2$ is the deformation tensor of $\overline{\mathbf{u}}$, and c_{ds} is computed using the dynamic procedure (Germano *et al.* 1991). The subgrid-scale vector is taken as $\sigma = \overline{\mathbf{u}\rho'} - \overline{\mathbf{u}}\,\overline{\rho'} = 0$, following fairly extensive tests of stratified mixing by Özgökmen *et al.* (2009a,b).

The domain is a $L\times L\times H$ box in x, y, z directions, respectively, with $L = 10^4$ m, and $H = 500$ m. Periodic boundary conditions are applied in the x direction, while free-slip, insulated walls are placed in the other directions. The initial condition is given by the analytical function

$$\rho'(\mathbf{x},0) = \left[1 - 0.7\left(\frac{z}{H}\right)^{2.3}\right] \left[1 - \exp\left\{-\left(\frac{y/L}{0.5+\epsilon}\right)^4 - \left(20\left(1-\frac{z}{H}\right)\right)^8\right\}\right], \tag{6}$$

which generates a $h_0 = 25$ m deep mixed layer and several km wide front perturbed by $\epsilon = 0.08\cos(2\pi\frac{x}{L}) + 0.03\cos(5\pi\frac{x}{L}) + 0.005\cos(20\pi\frac{x}{L}) + 0.01\cos(30\pi\frac{x}{L})$ (Figure 1a). The depth of the mixed layer is chosen to reflect h_0 in the Sargasso Sea in the summer, corresponding to the season of one of the ONR cruises. The turbulent exchange across the front, as quantified by an eddy diffusivity coefficient, is proportional to h_0^2 (Fox-Kemper *et al.* 2008). The wide range of wave lengths used in the perturbations reduce the spin-up time of the computation by letting the fast-growing modes emerge efficiently. The simulation is started from rest and contains no external (e.g. wind) forcing.

In selecting the parameters of the system, it is noted that values as high as $Re = 10^5$ and $Pe = 7\times10^5$ (and high resolution) are needed in order control vertical diffusion across the thin mixed layer. The other parameters are set to $Fr = 0.1$ and $Ro = 0.02$, as in Özgökmen *et al.* (2011). The fastest growing mode $\mathcal{R}$ in mixed layer instability is approximated by $R_d/\mathcal{R} \approx 0.2$ (Eldevik and Dysthe 2002), where $R_d = \sqrt{\frac{g}{\rho_0}\Delta\rho'_m\,h_0}/f$ is the radius of deformation in the mixed layer with $\Delta\rho'_m$ being the density change across the surface front. The number of largest coherent features that can fit in the domain is estimated from $\frac{L}{\mathcal{R}} \approx 0.2\,\frac{Fr}{Ro}\left(\frac{\Delta\rho'_m}{\Delta\rho'}\frac{h_0}{H}\right)^{-1/2}$.

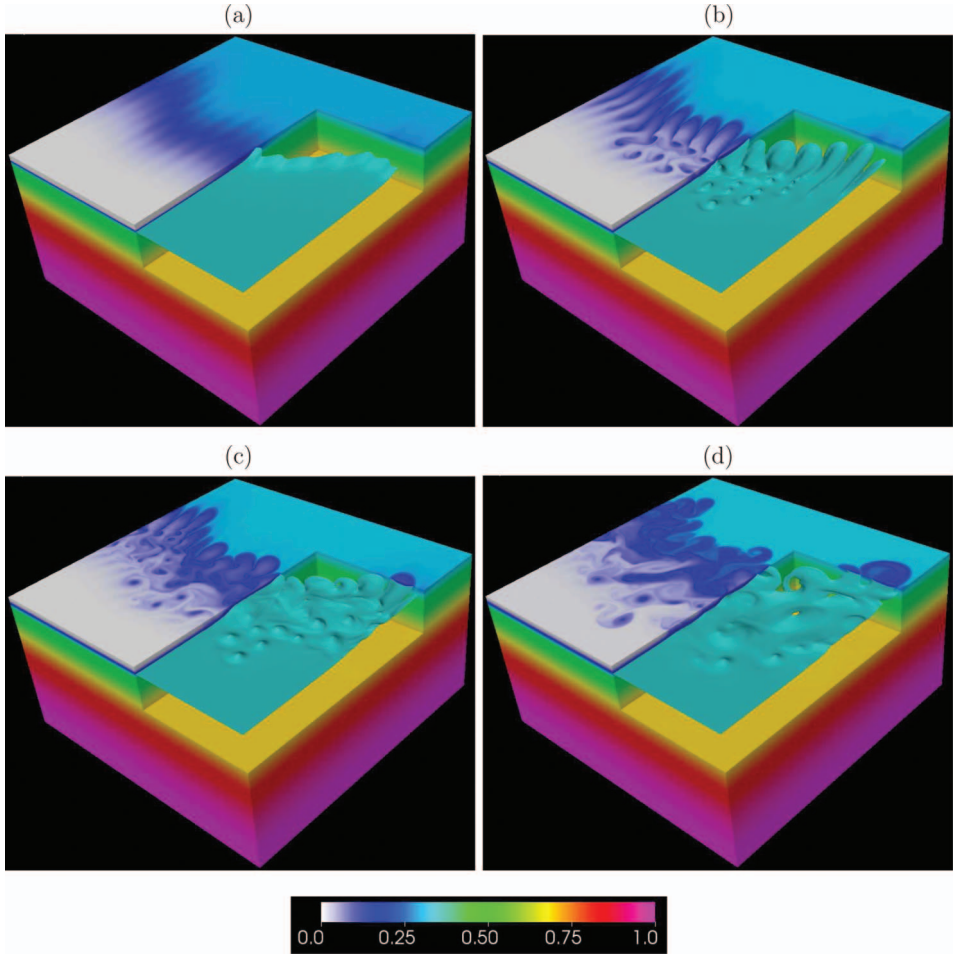

Figure 1. Perspective view of the density perturbation field ρ' at (a) $t=0$, (b) $t=11$ days, (c) $t=17.3$ days, and (d) $t=29.5$ days. The 3D plot is sliced in order to reveal the isopycnal at the base of the mixed layer. The surface plot shows the $\rho'=0.22$ isopycnal, marking the base of the mixed layer. The vertical axis is stretched 10 fold with respect to the realistic aspect ratio. The animation is available from: http://www.rsmas.miami.edu/personal/tamay/3D/mli116-tr.mov.

Substituting $\Delta\rho'_m/\Delta\rho' \approx 0.2$ and $h_0/H = 25/500$, we get $L/\mathcal{R} \approx 10$.

The domain is discretised using $K_x = K_y = 32$ and $K_z = 8$ elements in the horizontal and vertical directions, respectively. The horizontal elements have uniform spacing while those in the vertical are clustered near the mixed layer. On each element, solutions are represented by Legendre polynomials of order $\mathcal{N} = 11$, leading to the total number of grid points of $n = (K_x\mathcal{N}+1)(K_y\mathcal{N}+1)(K_z\mathcal{N}+1) = 11,090,201$. The Gauss–Labatto–Legendre quadrature points have a minimum and maximum spacings of $(\Delta x)_{\min} \approx \ell\frac{5}{\mathcal{N}^2}$ and $(\Delta x)_{\max} \approx \ell\frac{\pi}{2\mathcal{N}}$ for a given element length ℓ, resulting in 9 m $\leq \Delta x \leq$43 m and 0.4 m $\leq \Delta z \leq$1.8 m in the mixed layer. The computations are carried out on 128 processors using Virginia Tech's SystemX, as well as on IBM-P5 and Linux clusters at the University of Miami. The time step is equal to 150 s, for which the Courant number stays less than 0.4. The system is integrated for a total of about 29.5 days (about 17,000 steps), which takes a wall clock time of 24 h.

3. Results

3.1. *Description of the flow field*

From the initial perturbation ε consisting of various wavelengths, modes consistent with the scale of $\mathcal{R}$ grow fastest and towards the higher ρ' (northern side) of the front during the first week of the instability (Figure 1a,b). The circulation inside these modes is anticyclonic (clockwise or negative relative vorticity, ζ). Under the assumption that tilting/twisting and solenoidal terms in the vorticity budget are negligible, the potential vorticity (PV) can be expressed as $q = (f+\zeta)/h$, so that the initial PV in the mixed layer is $q_1 = f/h_0$. During the rotating gravitational adjustment, the water parcels in the mixed layer are advected such that their height h_1 reduces. Under the PV conservation $q^1 = f/h_0$ $(f+\zeta_1)/h$. Since

$h_1 < h_0, \zeta_1 < 0$, or anticyclonic circulation must develop inside these features. The zones in between these modes are subject to shear of reverse direction (cyclonic), which is also supported by PV conservation arguments for the deeper layer; $q_2 = f/(H - h_0) = (f + \zeta_2)/h_2$. Since $h_2 < (H - h_0)$, one gets $\zeta_2 > 0$. We note that the shear layers between the fastest growing surface modes continue to release small cyclonic vortices, that populate the mixed layer base (Figures 1b and 3b). There are occasional indications of Kelvin-Helmholtz type shear instability between the surface modes (Figure 1c). The weaker yet persistent geostrophic current caused by the front (from left to right of the domain, or with the deeper, high pressure perturbation pool on its right) appears to influence the flow evolution. First, it tends to disrupt the fastest growing modes, causing detachment of anticyclonic surface eddies. At longer times, anticyclonic surface eddies spin down, and the cyclonic shear along the northern side of the front creates a large number (about 10) of cyclonic spiraling eddies near the surface. Spiral eddies are commonly observed in the ocean, and their formation in this simulations appears to be consistent with the mechanism outlined in Figure 34 of Munk *et al.* (2000).

3.2. Sampling with passive scalars

Realistic size tracer strips are used to sample the mixed layer base. One of the striking first impressions is how small the dye patches are with respect to the submesoscale features in the flow field (Figure 2). Subsequently, multiple patches need to be considered, and positioning of the patches could play an important role given the limited observation period. It is assumed that the topology of the mixed layer base can be mapped to some degree of accuracy using ship board and/or profiling instruments. Two types of features are selected. The first type of features are centers of eddies that populate the mixed layer base (Figure 2a). These are essentially elliptic stagnation points that tend to trap particles. The second type of features are regions in between the eddies that are hyperbolic due to strain exerted by the eddies (Figure 2b). In order to accelerate the formation of tracer patterns, 10 patches of tracers are launched in a cross configuration (five independent locations) at the mixed layer base at 25 m. The launch time is chosen to be $t = 17.3$ days (Figure 1c), at which point the system exhibits well-developed instabilities, while allowing adequate time for integration before the closed boundaries influence the turbulent features.

Figure 2c,d indicates that rotation and trapping associated with the elliptic eddies, and stretching along the out-flowing manifolds of hyperbolic regions in between the eddies are apparent in the tracer fields sampled after 36 h. This result shows the feasibility of identifying some of the pronounced features in the mixed layer base using well-resolved sampling of dye, despite the translation of features by several km over the observation period.

Nevertheless, one of the primary obstacles associated with dye measurements is that the concentration field C is not easy to convert into useful diagnostics of transport. For instance, while the dye behaviour in Figure 2 is qualitatively indicative of elliptic and hyperbolic regimes in the underlying flow field, we are not aware of any quantitative methods of how to convert C into eigenvalues of the velocity gradient tensor, or compute components of strain tensor. This is mainly due to two reasons. First, dye parcels cannot be tagged (apart from using drifters), and second, formation of gradients in the dye field by the action of coherent features starts to become compensated by diffusion in Equation (4) at some point, most notably along the exponentially stretching (hyperbolic) branches of the flow field. It is common to compute second moment, or spreading around the center of mass from tracer measurements (Sundermeyer and Ledwell 2001). But it is not clear to us how to handle this in the spreading is highly anisotropic and only a small fraction of the turbulent features are sampled as in Figure 2. Comparison of tracer and particle horizontal position variances and extension to vertical diffusivity was presented in Figures 19 and 23 of Özgökmen *et al.* (2011). We have computed the following metric, $\chi^2(t) = \int |\nabla C(\mathbf{x}, t)|^2 \, dV / \int |C(\mathbf{x}, t)|^2 \, dV$, introduced by Pattanayak (2001) and Sundaram *et al.* (2009) to quantify this competition between chaotic advection and diffusion, but found no significant difference between the elliptic and hyperbolic launches during the anticipated 36 h, and even after the maximum 120 h of observation period.

3.3. Sampling with passive particles

The main disadvantage of drifters with respect to tracers is that they provide sparse information, as it is not feasible to release thousands of them in ocean experiments, given present technology. Nevertheless, particles offer two advantages over tracers. They are not subject to diffusion, and they provide position information, from which it is quite easy to compute quantities relevant to transport. A diagnostic of interest is the scale-dependent Lyapunov exponent (Finite Scale Lyapunov Exponents (FSLE), Artale *et al.* 1997, Aurell *et al.* 1997), which is directly connected to turbulent and scalar fluctuations in the underlying flow field:

$$\lambda(\delta) = \frac{\ln(\alpha)}{\langle \tau(\delta) \rangle}, \tag{7}$$

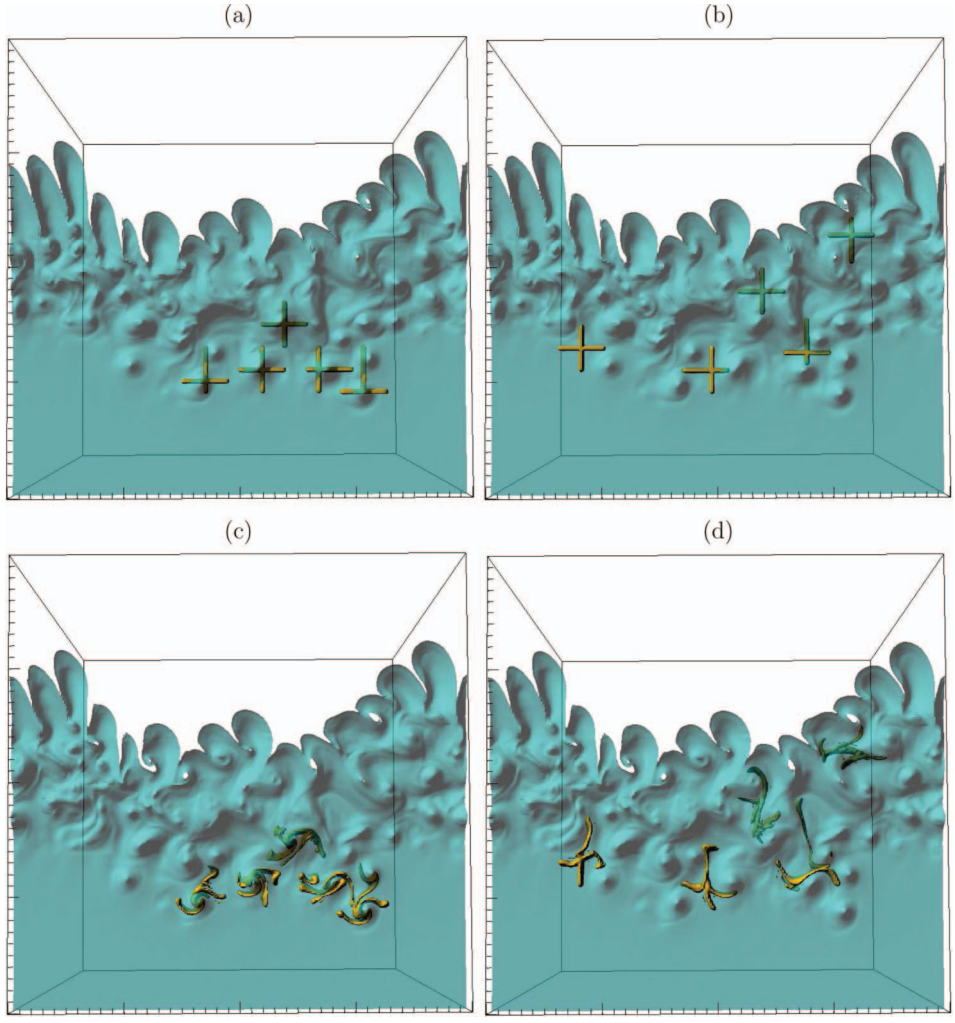

Figure 2. Top view of the domain showing the initial locations of realistic size tracer strips in cross configuration positioned to sample (a) eddies in the mixed layer base, and (b) regions in between the eddies. The surface plot shows the $\rho' = 0.22$ isopycnal, marking the base of the mixed layer, at $t = 17.3$ days. The vertical axis is stretched 30 fold to emphasise the turbulent coherent features. The state of the tracer strips (contoured using 0.1 within non-dimensional range of $0 \leq C \leq 1$) after 36 h are depicted in (c) and (d). The animations are available from: http://www.rsmas.miami.edu/personal/tamay/3D/mli121-tr-v1.mov and http://www.rsmas.miami.edu/personal/tamay/3D/mli122-tr-v1.mov.

where $\langle \tau(\delta) \rangle$ is the averaged time (over the number of particle-pairs) required to separate from a distance of δ to $\alpha\delta$. The FSLE has been used in many recent studies of oceanic dispersion (Lacorata *et al*. 2001, LaCasce and Ohlmann 2003, Haza *et al*. 2008, Koszalka *et al*. 2009, Haza *et al*. 2010, Lumpkin and Elipot 2010, Poje *et al*. 2010, Schroeder *et al*. 2011).

In order to obtain an accurate evaluation of $\lambda(\delta)$ in this flow simulation, the field is sampled over an area of 2 km × 5.5 km using 3528 particles launched as triplets at 25 m depth (Figure 3a). The particles composing the triplets are released 20 m apart, and the triplets are 100 m apart. Particles are advected online for about 30 days with the model time step of 150 s, while the positions are recorded at 30 min intervals, as per observational requirements.

The resulting $\lambda(\delta)$ plot (Figure 4) identifies a constant-value plateau for the scale separation range from 20 m $\leq \delta \leq$ 600 m and a fall off to Richardson regime for larger separation distances. The fall-off scale is related to the average eddy diameter in the sampled field, while the value of the maximum FSLE is the average stretching that the particles experience (Poje *et al*. 2010). The maximum value seems to be about $\lambda_{\max} \approx 0.4$ days^{-1}. Estimates from the observational and modelling studies listed above are in the range of $0.3 \leq \lambda_{\max} \leq 10$ days^{-1}. The present value is on the lower end of the spectrum of estimates, primarily because all others are for near-surface flows. A previous study on mixed layer LES (Özgökmen *et al*. 2011) revealed a maximum Lyapunov exponent $\lambda_{\max} \approx$ 2 days^{-1}, with the primary differences being that the

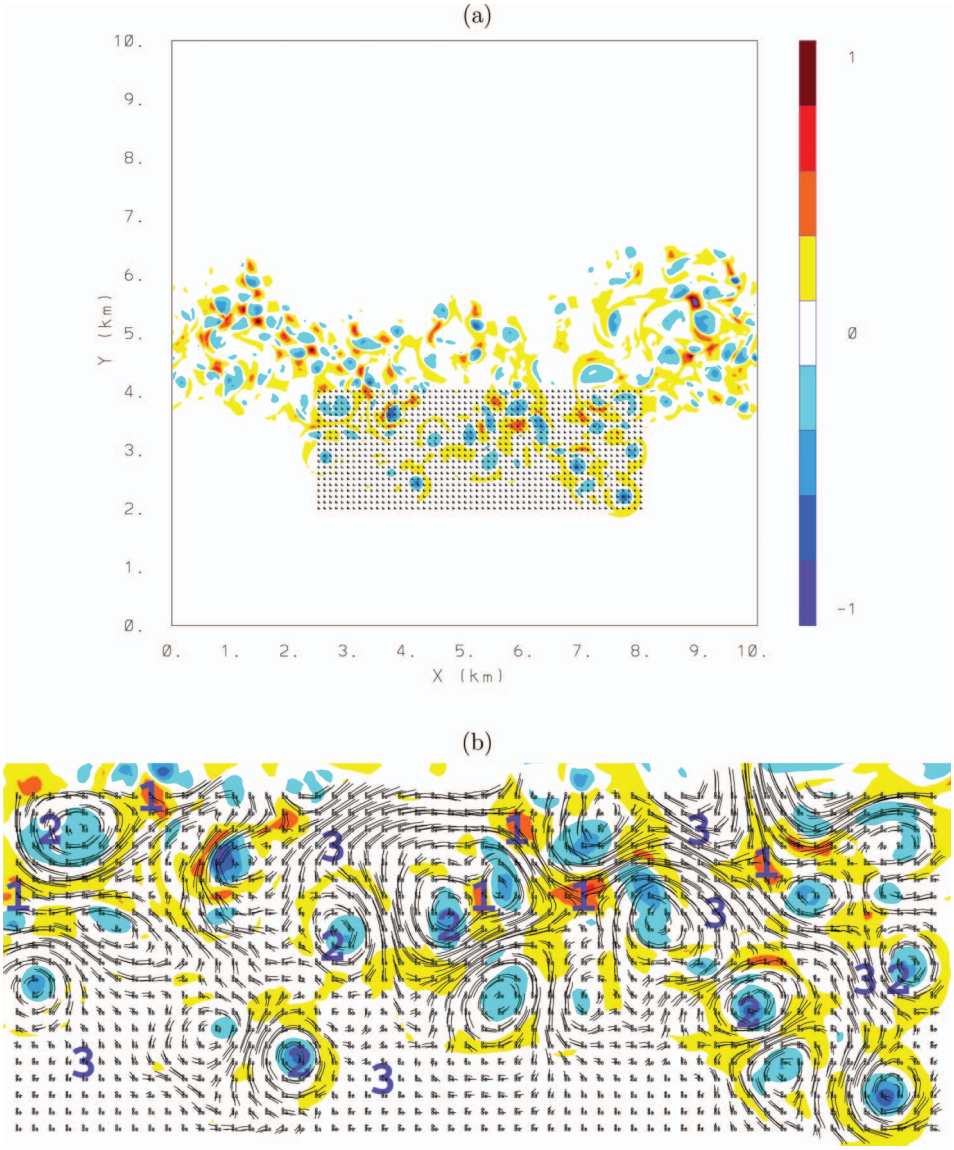

Figure 3. (a) Okubo–Weiss (OW) parameter, normalised by midlatitude Coriolis parameter ($f = 7 \times 10^{-5}$ s^{-1}), Q'/f^2, at 25 m depth and $t = 17.3$ days, as well as initial positions of 3528 particles launched in triplets. (b) Targeted launches of triplets in six strain dominated regions ($Q' > 0$, marked with '1'), in six vorticity dominated regions ($Q' < 0$, marked with '2') and six regions of low Q' (marked with '3').

instability of a thicker ($h_0 = 80$ m) mixed layer was sampled at 5 m depth.

Then, the following question is posed:

- How do we target a much smaller number of particles (18) to approximate this $\lambda(\delta)$ curve with the least error?

It is helpful to use a quantitative criterion to select the target areas. Here we employ the Okubo–Weiss (OW) criterion (Okubo 1970, Weiss 1991), $Q = S^2 - \omega^2 = \left(\frac{\partial u}{\partial x} + \frac{\partial v}{\partial y}\right)^2 + 4\left(\frac{\partial u}{\partial y}\frac{\partial v}{\partial x} - \frac{\partial u}{\partial x}\frac{\partial v}{\partial y}\right)$, where $S^2 = \left(\frac{\partial u}{\partial x} - \frac{\partial v}{\partial y}\right)^2 + \left(\frac{\partial v}{\partial x} + \frac{\partial u}{\partial y}\right)^2$ is the square of the horizontal strain rate, $\omega^2 = \left(\frac{\partial v}{\partial x} - \frac{\partial u}{\partial y}\right)^2$ the square of horizontal vorticity. The OW criterion is a useful Eulerian metric to differentiate the hyperbolic ($Q > 0$) and elliptic ($Q < 0$) parts of a two-dimensional flow field. It is assumed that data from other *in situ* instruments can help construct an approximate OW map to help guide targeted drifter launches. The construction of an OW map is a challenging task using ship-board instruments, since this requires a synoptic view of the horizontal velocity field. But it is not impossible if two or more ships follow parallel tracks with a good sense

of aliasing errors, or if several dozens of profiling floats are employed. Contamination of the signal associated with the coherent features by the internal wave field could also be another issue that is likely to be encountered in the field. For further simplicity, only the non-divergent part of the OW is used, $Q' = 4(\frac{\partial u}{\partial y}\frac{\partial v}{\partial x} - \frac{\partial u}{\partial x}\frac{\partial v}{\partial y})$. Scaling with a midlatitude Coriolis frequency shows that extrema of $|Q'|/f^2$ are on the order of 1 (Figure 3a), indicative of high strain and vorticity values characteristic of submesoscale flows (Thomas *et al*. 2008).

A set of five targeted releases are carried out (Figure 3b). The first release contains six triplets at strain-dominated regions ($Q' > 0$, between eddies), the second in elliptic regions ($Q' > 0$, inside eddies), and the third in $Q' \approx 0$ regions. The fourth and fifth launches contain two realisations of random combinations consisting of two of each type of release (so-called mixed releases).

Figure 4 shows that the first launch starts with high FSLE (as expected) but drops almost to the true curve (from 3528 particles) at $\delta \approx 100$ mm, which seems to be the scale that the particles remain inside high strain initial regions. The launches in region two show low FSLE up to $\delta \approx 600$ mm (the average size of the eddies, as expected). The mixed launches are possibly the best performing. Nevertheless, perhaps the main message is that almost all of the releases are leading to quite accurate results, because there are many eddies and high hyperbolicity in the mixed layer base, and given enough time, 18 particles seem to sample the dispersive statistics of these features quite satisfactorily.

While particle/tracer variances are accurate measures of how the turbulent exchange widens an ocean front, they may not be necessarily the best measures of submesoscale features which tend to lead to rapidly stretching filaments, in a significant deviation from a diffusive processes. The scale-dependent FSLE presented in the manuscript is an accurate statistical measure of the strain rate ($\lambda_{\max}$) induced by submesoscale eddies, and their scale (approximate width of the FSLE plateau). As Figure 4 indicates, the regimes of the $\lambda(\delta)$ are super diffusive at all separation scales.

4. Summary and future directions

The primary original aspects of this study and our main findings are highlighted below. Several comments on the future of CFD-based approaches in ocean modelling follow.

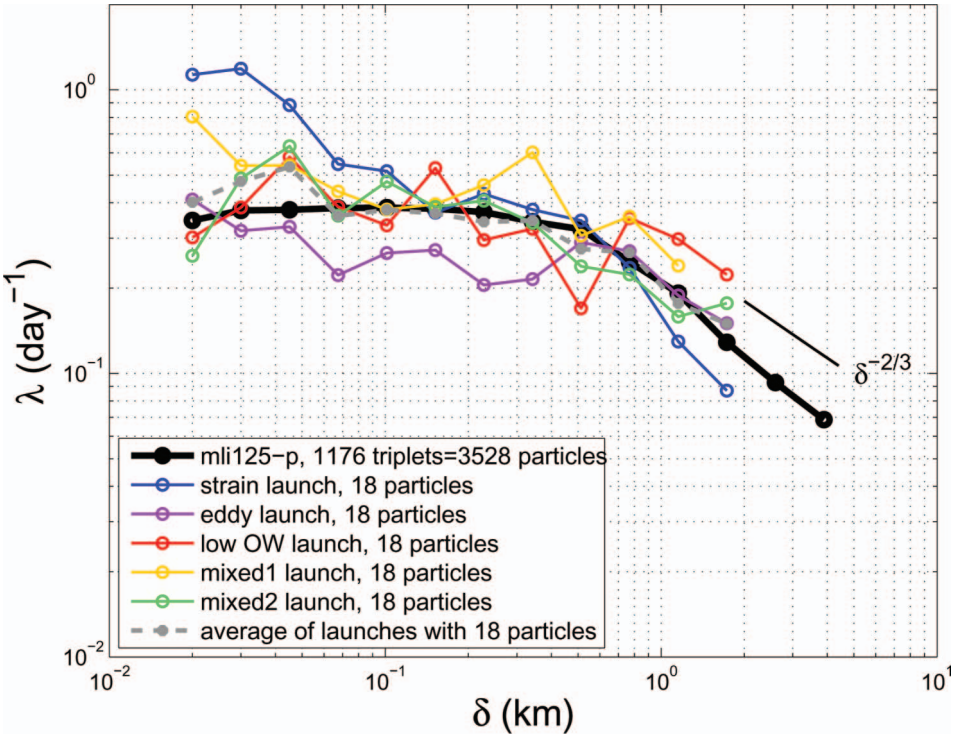

Figure 4. The scale-dependent FSLE $\lambda(\delta)$ from the full set with 3528 particles, and targeted sets each with 18 particles. The average FSLE from five launches with 18 particles is also shown. The slope in the background indicates the Richardson dispersion regime ($\lambda \sim \delta^{-2/3}$).

(a) To our knowledge, this is the first numerical study in which such shallow mixed layer instabilities have been explicitly resolved, primarily due to lack of numerical dissipation of the high-order numerical model. In addition, the high resolution of the model allows the simulation of realistic size tracer patches. Both aspects highlight some of the capabilities of CFD-based ocean modelling approaches over more conventional, parameterisation-based avenues.
(b) Our results put the use of realistic-size tracers in perspective. Larger amounts and/or longer observing periods than those used here seem to be preferable to sample the eddies at the mixed layer base. Alternatively, if ocean experiments indicate much larger rates of tracer spreading than those observed here, then this would imply the importance of missing processes in our idealised configuration.
(c) We conclude that the results presented here are supportive of the effectiveness of Lagrangian drifters in sampling rapidly evolving submesoscale mixed layer flows. Future availability of cheaper, smaller and environmentally degradable drifters may permit their deployment in large numbers [on the O(100)] for better observing capabilities.
(d) To our knowledge, this is one of the few computations in which spiral eddies, often observed in the ocean (Munk *et al.* 2000), emerge spontaneously. We provide support to the idea put forward by Eldevik and Dysthe (2002) that spiral eddies originate from frontal instabilities at the ocean's mixed layer.
(e) We also provide a brief overview of how CFD-based approaches can contribute to ocean modelling and *in situ* sampling.

Presently, LES and OGCMs are fully complementary in that LES models provide more reliable results for scales smaller than the submesoscales, while OGCMs contain realistic mesoscale currents and general circulation. Both modelling approaches overlap over the submesoscale range. It is not a practical long-term solution to try to couple an LES model to OGCMs due to large differences in their architecture. The discontinuity between BE and PE sets is most notable when considering such multi-scale simulations. Assuming a steady growth in computing power, we envision a hard barrier for OGCMs at about the submesoscale range, while LES models can continue to expand their frontier towards larger scales. Certainly, adaptive mesh refinement (AMR) methods within FEM/SEM can be used for multi-scale simulations (Mavriplis 1994). A hybrid approach is to solve BE over a finer mesh and computationally cheaper PE over coarser mesh regions of the domain within the same code (Botelho *et al.* 2009). Nevertheless, assuming that about half of the mesh points are dedicated to coarse grid parts of the domain, a speed up factor of at most two does not encourage dealing with potentially complex dynamical mismatches arising from different equation sets in the same domain. A third idea is to find intermediate equation sets which smoothly bridge the BE and PE (Duan *et al.* 2010). But, such approaches have not been tested yet. Therefore, a reasonable avenue for a multi-scale ocean modelling system is to rely only on LES codes, like Nek5000, for which we do not see any major complications regarding future development. Perhaps one aspect that will gain increasingly more attention is the post-analysis of large outputs that will be inevitably generated by multi-scale computations. It will not always be possible to estimate *a priori* which measures are of interest for a specific problem. Running the scalable main code on a large number of cores multiple times is likely to be more efficient for generating on-line diagnostic metrics than using off-line post-processing tools on a smaller number of processors.

Acknowledgements

We greatly appreciate the support of the Office of Naval Research and National Science Foundation via grants N00014-09-1-0267, DMS-1025323, DMS-1025359 under the Collaborative Mathematics and Geoscience (CMG) initiative. This research was made possible in part by a grant from BP/The Gulf of Mexico Research Initiative. We thank all members of the Lateral Mixing DRI team, who have provided guidance through many insightful comments. The computations were carried out on the University of Miami's high-performance computing (HPC) center (http://ccs.miami.edu/hpc/), on SystemX at Virginia Tech's advanced research computing center (http://www.arc.vt.edu) and at the City University of New York High Performance Computing Center under NSF Grants CNS-0855217 and CNS-0958379. We thank the four anonymous reviewers whose comments resulted in a significant improvement of the manuscript. We greatly appreciate the leadership of Catherine Mavriplis in organising this timely special issue, and many useful comments and guidance she provided during the preparation of this manuscript.

Notes

1. http://www.hycom.org/ocean-prediction
2. http://nek5000.mcs.anl.gov/index.php/Main_Page
3. http://www.aviso.oceanobs.com/es/data/products/index.html
4. http://oceancolor.gsfc.nasa.gov/cgi/image_archive.cgi?c=CHLOROPHYLL

References

Artale, V., *et al.*, 1997. Dispersion of passive tracers in closed basins: beyond the diffusion coefficient. *Physics Fluids*, 9, 3162–3171.

Aurell, E., *et al*., 1997. Predictability in the large: an extension of the concept of Lyapunov exponent. *Journal of Physics A*, 30, 1–26.

Baumert, H. and Peters, H., 2004. Turbulence closure, steady state, and collapse into waves. *Journal of Physical Oceanography*, 34, 505–512.

Baumert, H., Simpson, J., and Sündermann, J., 2005. *Marine turbulence*. Cambridge, UK: Cambridge University Press.

Boccaletti, G., Ferrari, R., and Fox-Kemper, B., 2007. Mixed layer instabilities and restratification. *Journal of Physical Oceanography*, 37, 2228–2250.

Botelho, D., *et al*., 2009. A hydrostatic/non-hydrostatic grid-switching strategy for computing high-frequency, high wave number motions embedded in geophysical flows. *Environmental Modelling and Software*, 24, 473–488.

Burchard, H. and Baumert, H., 1995. On the performance of a mixed-layer model based on the $k-\varepsilon$ turbulence closure. *Journal of Geophysical Research*, 100, 8523–8540.

Burchard, H. and Bolding, K., 2001. Comparative analysis of four second-moment turbulence closure models for the oceanic mixed layer. *Journal of Physical Oceanography*, 31, 1943–1968.

Canuto, V., Cheng, Y., and Howard, A., 2007. Non-local ocean mixing mode and a new plume model for deep convection. *Ocean Modelling*, 16, 28–46.

Canuto, V.M., *et al*., 2001. Ocean turbulence. Part i: one-point closure model momentum and heat vertical diffusivities. *Journal of Physical Oceanography*, 31, 1413–1426.

Capet, X., *et al*., 2008. Mesoscale to submesoscale transition in the California Current System: I flow structure, eddy flux and observational tests. *Journal of Physical Oceanography*, 38, 29–43.

Chang, Y., *et al*., 2005. Comparison of gravity current mixing parameterizations and calibration using a high-resolution 3d nonhydrostatic spectral element model. *Ocean Modelling*, 10, 342–368.

Davis, R., 1985. Drifter observations of coastal currents during CODE. The method and descriptive view. *Journal of Geophysical Research*, 90, 4741–4755.

Deville, M., Fischer, P., and Mund, E., 2002. High-order methods for incompressible fluid flow. *Vol. 9 of cambridge monographs on applied and computational mathematics*. Cambridge, UK: Cambridge University Press.

Duan, J., *et al*., 2010. Bridging the Boussinesq and primitive equations through spatio-temporal filtering. *Applied Mathematics Letters*, 23, 453–456.

Eldevik, T., and Dysthe, K., 2002. Spiral eddies. *Journal of Physical Oceanography*, 32, 851–869.

Ferziger, J., 2005. Direct and large-eddy simulation of turbulence. *In*: H.Z. Baumert, J.H. Simpson and J. Sündermann, eds. *Marine turbulence – theories, observations and models*. Cambridge, UK: Cambridge University Press, 160–181.

Fox-Kemper, B., Ferrari, R., and Hallberg, R., 2008. Parameterization of mixed-layer eddies. Part i: theory and diagnosis. *Journal of Physical Oceanography*, 38, 1145–1165.

Garrett, C. and Munk, W., 1972. Space-time scales of internal waves. *Geophysical Fluid Dynamics*, 2, 225–264.

Germano, M., *et al*., 1991. A dynamic subgrid-scale eddy viscosity model. *Physics Fluids A*, 3, 1760–1765.

Haza, A.C., *et al*., 2008. Relative dispersion from a high-resolution coastal model of the Adriatic Sea. *Ocean Modelling*, 22, 48–65.

Haza, A., *et al*., 2010. Transport properties in small scale coastal flows: relative dispersion from VHF radar measurements in the Gulf of La Spezia. *Ocean Dynamics*, 60, 861–882.

Ilicak, M., *et al*., 2008. Performance of two-equation turbulence closures in three-dimensional simulations of the Red Sea overflow. *Ocean Modelling*, 24, 122–139.

Ilicak, M., *et al*., 2009. Non-hydrostatic modeling of exchange flows across complex geometries. *Ocean Modelling*, 29, 159–175.

Kantha, L.H. and Clayson, C.A., 1994. An improved mixed layer model for geophysical applications. *Journal of Geophysical Research*, 99, 25235–25266.

Kantha, L.H. and Clayson, C.A., 2000. *Small scale processes in geophysical flows*. New York, NY: Academic Press.

Kaplan, D., Largier, J., and Botsford, L., 2005. HF radar observations of surface circulation off Bodega Bay (northern California, USA). *Journal of Geophysical Research*, 110, doi: 10.1029/2005JC002959.

Klein, P. and Lapeyre, G., 2009. The oceanic vertical pump induced by mesoscale and submesoscale turbulence. *Annual Review of Marine Science*, 1, 351–375.

Koszalka, I., LaCasce, J.H., and Orvik, K.A., 2009. Relative dispersion statistics in the Nordic Seas. *Journal of Marine Research*, 67, 411–433.

LaCasce, J.H. and Ohlmann, C., 2003. Relative dispersion at the surface of the Gulf of Mexico. *Journal of Marine Research*, 61 (3), 285–312.

Lacorata, G., Aurell, E., and Vulpiani, A., 2001. Drifter dispersion in the Adriatic sea: Lagrangian data and chaotic model. *Annales Geophysicae*, 19, 121–129.

Large, W., 1998. Modeling and parameterizing the ocean planetary boundary layer. *In*: E.P. Chassignet and J. Verron, eds. *Ocean modeling and parameterization*. Dordrecht, The Netherlands: Kluwer Academic Publishers, 81–120.

Lumpkin, R. and Elipot, S., 2010. Surface drifter pair spreading in the North Atlantic. *Journal of Geophysical Research C: Oceans*, 115, C12017.

Lumpkin, R. and Pazos, M., 2007. Measuring surface currents with Surface Velocity Program drifters: the instrument, its data, and some recent results. *In*: A. Griffa, A.D. Kirwan, A. Mariano, T. Özgökmen and T. Rossby, eds. Lagrangian analysis and prediction of coastal and ocean dynamics. Cambridge: Cambridge University Press, 39–67.

Maday, Y. and Patera, A.T., 1989. Spectral element methods for the Navier-Stokes equations. *In*: A.K. Noor, ed. *State of the art surveys in computational mechanics*. New York: ASME, 71–143.

Mahadevan, A. and Tandon, A., 2006. An analysis of mechanisms for submesoscale vertical motion at ocean fronts. *Ocean Modelling*, 14, 241–256.

Mavriplis, C., 1994. Adaptive mesh strategies for the spectral element method. *Computer Methods in Applied Mechanics and Engineering*, 116, 77–86.

McWilliams, J., 2008. Fluid dynamics at the margin of rotational control. *Environmental Fluid Mechanics*, 8, 441–449.

Mellor, G.L. and Yamada, T., 1982. Development of a turbulence closure model for geophysical fluid problems. *Reviews of Geophysics*, 30, 851–875.

Müller, P., McWilliams, J., and Molemaker, M., 2005. Routes to dissipation in the ocean: the two-dimensional/three-dimensional turbulence conundrum. *In*: H.Z. Baumert, J. Simpson and J. Sündermann, eds. *Marine turbulence: theories, observations, and models. Results of the CARTUM project*. Cambridge, UK: Cambridge University Press, 397–405.

Munk, W., *et al*., 2000. Spirals on the sea. *Proceedings of the Royal Society: London A*, 546, 1217–1280.

Ohlmann, J.C., *et al*., 2005. GPD-cellular drifter technology for coastal observing system. *Journal of Atmospheric and Oceanic Technology*, 22, 1381–1388.

Okubo, A., 1970. Horizontal dispersion of floatable particles in vicinity of velocity singularities such as convergences. *Deep-Sea Research*, 17 (3), 445–454.

Özgökmen, T. and Fischer, P., 2008. On the role of bottom roughness in overflows. *Ocean Modelling*, 20, 336–361.

Özgökmen, T., Fischer, P., and Johns, W., 2006. Product water mass formation by turbulent density currents from a high-order nonhydrostatic spectral element model. *Ocean Modelling*, 12, 237–267.

Özgökmen, T., Iliescu, T., and Fischer, P., 2009a. Large eddy simulation of stratified mixing in a three-dimensional lock-exchange system. *Ocean Modelling*, 26, 134–155.

Özgökmen, T., Iliescu, T., and Fischer, P., 2009b. Reynolds number dependence of mixing in a lock-exchange system from direct numerical and large eddy simulations. *Ocean Modelling*, 30, 190–206.

Özgökmen, T., *et al*., 2007. Large eddy simulation of stratified mixing in two-dimensional dam-break problem in a rectangular enclosed domain. *Ocean Modelling*, 16, 106–140.

Özgökmen, T., *et al*., 2011. Large eddy simulations of mixed layer instabilities and sampling strategies. *Ocean Modelling*, 39, 311–331.

Özgökmen, T.M., *et al*., 2004a. Three-dimensional turbulent bottom density currents from a high-order nonhydrostatic spectral element model. *Journal of Physical Oceanography*, 34 (9), 2006–2026.

Özgökmen, T.M., *et al*., 2004b. Entrainment in bottom gravity currents over complex topography from three-dimensional nonhydrostatic simulations. *Geophysical Research* Letters, 31 (L13212), doi: 10.1029/2004GL020186.

Paduan, J. and Rosenfeld, L., 1996. Remotely sensed surface currents in Monterey Bay from shore based HF radar (Coastal Ocean Dynamics Application Radar). *Journal of Geophysical Research*, 101/C9, 20669–20686.

Patera, A., 1984. A spectral element method for fluid dynamics: laminar flow in a channel expansion. *Journal of Computational Physics*, 54, 468–488.

Pattanayak, A., 2001. Characterizing the metastable balance between chaos and diffusion. *Physica D*, 148, 1–19.

Poje, A., *et al*., 2010. Resolution dependent relative dispersion statistics in a hierarchy of ocean models. *Ocean Modelling*, 31, 36–50.

Sanford, T., Kelly, K., and Farmer, D., 2011. Sensing the ocean. *Physics Today*, February, 24–28.

Schroeder, K., *et al*., 2011. Relative dispersion in the liguro-provencal basin: from sub-mesoscale to mesoscale. *Deep-Sea Research*, Part I, 58, 861–882.

Scotti, A., and Mitran, S., 2008. An approximated method for the solution of elliptic problems in thin domains: application to nonlinear internal waves. *Ocean Modelling*, 25, 144–153.

Shay, L., Cook, T., and An, P., 2003. Submesoscale coastal ocean flows detected by very high frequency radar and autonomous underwater vehicles. *Journal of Atmospheric and Oceanic Technology*, 20, 1583–1600.

Shay, L., *et al*., 2007. High-frequency radar mapping of surface currents using WERA. *Journal of Atmospheric and Oceanic Technology*, 24, 484–503.

Steward, R. and Joy, J., 1974. HF radio measurements of surface currents. *Deep-Sea Research*, 21, 1039–1049.

Sundaram, B., Poje, A., and Pattanayak, A., 2009. Persistent patterns and multifractality in fluid mixing. *Physical Review E*, 79, 066202.

Sundermeyer, M. and Ledwell, J., 2001. Lateral dispersion over the continental shelf: analysis of dye release experiments. *Journal of Geophysical Research*, 106, 9603–9621.

Sundermeyer, M., *et al*., 2007. Three-dimensional mapping of fluorescent dye using a scanning, depth-resolving airborne radar. *Journal of Atmospheric and Oceanic Technology*, 24, 1050–1065.

Thomas, L., Tandon, A., and Mahadevan, A., 2008. Submesoscale processes and dynamics. *In*: M. Hecht and H. Hasume, eds. *Ocean modeling in an Eddying Regime*, Vol. 177. Washington, D.C.: American Geophysical Union, Geophysical Monograph, 17–38.

Umlauf, L. and Burchard, H., 2005. Second-order turbulence closure models for geophysical boundary layers. a review of recent work. *Continental Shelf Research*, 25, 795–827.

Vallis, G., 2006. *Atmospheric and oceanic fluid dynamics*. Cambridge, UK: Cambridge University Press.

Warner, J.C., *et al*., 2005. Performance of four turbulence closure methods implemented using a generic length scale method. *Ocean Modelling*, 8, 81–113.

Webb, D., Simonetti, P., and Jones, C., 2001. SLOCUM: an underwater glider propelled by environmental energy. *IEEE Journal of Oceanic Engineering*, 26, 447–452.

Weiss, J., 1991. The dynamics of enstrophy transfer in 2-dimensional hydrodynamics. *Physica D*, 48 (2–3), 273–294.

Wilcox, D., 1998. *Turbulence modeling for CFD*. 2nd ed. La Canada, CA: DCW Industries, Inc.

Wunsch, C. and Ferrari, R., 2004. Vertical mixing, energy, and the general circulation of the oceans. *Annual Review of Fluid Mechanics*, 36, 281–314.

Xu, X., *et al*., 2006. Parameterization of gravity current entrainment for ocean circulation models using a high-order 3d nonhydrostatic spectral element model. *Ocean Modelling*, 14, 19–44.